On the Origin of the Elliptic Flow and its Dependence on the Equation of State in Heavy Ion Reactions at Intermediate Energies

A. Le Fèvre[1], Y. Leifels[1], C. Hartnack[2] and J. Aichelin[2]
[1] *GSI Helmholtzzentrum für Schwerionenforschung GmbH, Planckstr. 1, 64291 Darmstadt, Germany and*
[2] *SUBATECH, Université de Nantes, EMN, IN2P3/CNRS*
4 rue Alfred Kastler, 44307 Nantes cedex 3, France
(Dated: November 23, 2016)

Recently it has been discovered that the rapidity dependence of the elliptic flow, v_2, of charged particles shows the strongest sensitivity to the Nuclear Equation of State (EoS) which has been observed within a microscopic model. This dependence on the nuclear EoS is predicted by Quantum Molecular Dynamics (QMD) calculations [1] which show as well that the absorption or rescattering of in-plane emitted particles by the spectator matter is not the main reason for the EoS dependence of the elliptic flow at mid-rapidity.The reason are different density gradients (and therefore different forces) in the direction of the impact parameter (x-direction) as compared to the direction perpendicular to the reaction plan (y-direction), due to the presence of the spectator matter.

The stronger density gradient in y-direction accelerates the particles more and creates therefore a negative v_2.

arXiv:1611.07500v1 [nucl-th] 22 Nov 2016

I. INTRODUCTION

The elliptic flow at midrapidity, originally called out-of-plane emission or squeeze-out, has attracted a lot of attention during the last years. It has been predicted in hydrodynamical simulations of heavy ion reactions [2–4] and has later been found experimentally by the Plastic Ball collaboration [5].

The elliptic flow is described by the second moment of the Fourier expansion of the azimuthal distribution of the emitted particles with respect to the reaction plane and along the beam axis.

$$\frac{d\sigma(y)}{d\phi} = C(1 + 2v_1(y)\cos\phi + 2v_2(y)\cos 2\phi.....) \qquad (1)$$

A positive v_2-value characterizes elliptic flow in the reaction plane and a negative value out-of plane flow. For symmetry reasons v_1 becomes zero at midrapidity and therefore v_2 can be determined directly from experiment. At ultra-relativistic energies the measured elliptic flow and its centrality dependence has been considered as an experimental proof that during the expansion of the system the almond shaped initial spatial configuration of the overlap region is transformed into an elliptic flow with a *positive* v_2 value, which is predicted by viscous hydrodynamics [6]. At lower energies the E895 Collaboration [7] and especially the FOPI collaboration [8] have investigated elliptic flow and found a *negative* v_2 coefficient up to beam energies of ≈ 6 AGeV with a minimum at around 0.4-0.6 AGeV [9, 10]. These results are compiled in Fig. 1. Therefore, the elliptic flow has to be of a different origin at these energies. It has been suggested in [11] that the v_2 value is negative at these energies because the compressed matter expands while spectator matter is still present and blocks the in-plane emission. At higher incident energies the expansion takes place after the spectator matter has passed the compressed zone and therefore the elliptic flow is determined by the shape of the overlap region only. This leads to a positive v_2.

Recently the FOPI collaboration has analyzed its experimental findings in the framework of Quantum Molecular Dynamics (QMD) calculations [1] and has concluded that elliptic flow at energies between 0.2 and 2.0 AGeV has the largest dependence on the stiffness of the nuclear EoS, an even larger dependence than found earlier for the production of K^+ mesons [12, 14]. This came as a surprise because blocking of the in-plane emission by spectator matter should show only a moderate dependence on the compressibility of the nuclear EoS. These findings created therefore a renewed interest to study in detail the origin of the elliptic flow and its dependence on the EoS. In this article we report on these investigations. In section 2 we will shortly introduce the Quantum Molecular Dynamics (QMD) approach which we use for the analysis. Section 3 is devoted to a survey of the reaction, especially to a comparison of the reaction scenarios for different EoS. In section 4 we study in detail the elliptic flow created in these reaction and analyze its origin and its EoS dependence. We summarize our work in section 5.

II. THE QUANTUM MOLECULAR DYNAMICS APPROACH

The details of the Quantum Molecular Dynamics (QMD) approach have been published in [13–15]. Here, we repeat only how this approach allows for an exploration of the nuclear EoS.

In the QMD approach nucleons are presented as Gaussian wave functions. A generalized Ritz variational principle allows to determine the time evolution of the centroids of the Gaussians in coordinate and momentum space.

$$\dot{r_i} = \frac{\partial\langle H\rangle}{\partial p_i} \qquad \dot{p_i} = -\frac{\partial\langle H\rangle}{\partial r_i} \quad , \qquad (2)$$

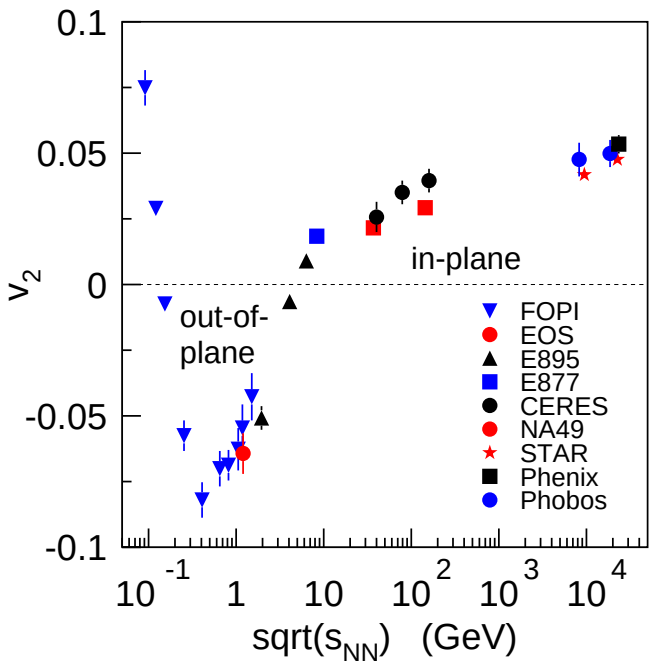

FIG. 1. (Color online) Elliptic flow v_2 at mid-rapidity as a function of the incident energy measured in semi-central Au+Au collisions by various experiments, indicated by the different symbols. Data extracted from refs. [7, 9–11]

where the expectation value of the total Hamiltonian is

$$\begin{aligned}\langle H\rangle &= \langle T\rangle + \langle V\rangle \\ &= \sum_i \frac{p_i^2}{2m_i} + \sum_i \sum_{j>i} \int f_i(\mathbf{r},\mathbf{p},t)\, V(\mathbf{r},\mathbf{r}',\mathbf{p},\mathbf{p}') \\ &\cdot\ f_j(\mathbf{r}',\mathbf{p}',t)\, \mathrm{d}\mathbf{r}\, \mathrm{d}\mathbf{r}' \mathrm{d}\mathbf{p}\, \mathrm{d}\mathbf{p}' \quad . \end{aligned} \tag{3}$$

f_i is the single-particle Wigner density

$$f_i(\mathbf{r},\mathbf{p},t) = \frac{1}{\pi^3\hbar^3} \mathrm{e}^{-\frac{2}{L}(\mathbf{r}-\mathbf{r_i}(t))^2} \mathrm{e}^{-\frac{L}{2\hbar^2}(\mathbf{p}-\mathbf{p_i}(t))^2} \quad . \tag{4}$$

The potential consists of several terms:

$$\begin{aligned} V(\mathbf{r_i},\mathbf{r_j},\mathbf{p_i},\mathbf{p_j}) &= G + V_{\mathrm{Coul}} \\ &= V_{\mathrm{Skyrme}} + V_{\mathrm{Yuk}} + V_{\mathrm{mdi}} + + V_{sym} + V_{\mathrm{Coul}} \\ &= t_1\delta(\mathbf{r_i}-\mathbf{r_j}) + t_2\delta(\mathbf{r_i}-\mathbf{r_j})\rho^{\gamma-1}(\mathbf{r_i}) + \\ &\quad t_3 \frac{\exp\{-|\mathbf{r_i}-\mathbf{r_j}|/\mu\}}{|\mathbf{r_i}-\mathbf{r_j}|/\mu} + \\ &\quad t_4 \ln^2(1+t_5(\mathbf{p_i}-\mathbf{p_j})^{\mathbf{2}})\delta(\mathbf{r_i}-\mathbf{r_j}) + \\ &\quad t_6 \frac{1}{\varrho_0} T_3^i T_3^j \delta(\mathbf{r_i}-\mathbf{r_j}) + \frac{Z_i Z_j e^2}{|\mathbf{r_i}-\mathbf{r_j}|}. \end{aligned} \tag{5}$$

The total one-body Wigner density is the sum of the Wigner densities of all nucleons. The nuclear EoS, on the other hand, describes the properties of infinite nuclear matter (without Coulomb interactions) and is therefore given by the volume energy only. The EoS describes the variation of the energy $E(T=0,\rho/\rho_0)$ when changing the nuclear density to values different from the saturation density ρ_0 for zero temperature. Often nuclear matter is assumed to be isospin saturated, but we also consider asymmetric nuclear matter, where the symmetry energy term contributes.

The single-particle potential resulting from the convolution of the distribution functions f_i and f_j with the interactions $V_{\mathrm{Skyrme}} + V_{\mathrm{mdi}}$ (local interactions including their momentum dependence) is for symmetric nuclear matter

$$U_i(\mathbf{r_i},t) = \alpha\left(\frac{\rho_{int}}{\rho_0}\right) + \beta\left(\frac{\rho_{int}}{\rho_0}\right)^{\gamma} + \delta \ln^2\left(\varepsilon\,(\Delta\mathbf{p})^2+1\right)\left(\frac{\rho_{int}}{\rho_0}\right) \quad , \tag{6}$$

where ρ_{int} is the interaction density obtained by convoluting the distribution function of a particle with the distribution functions of all other particles of the surrounding medium. $\Delta\mathbf{p}$ is the relative momentum of a particle with respect to the surrounding medium.

In nuclear matter the parameters t_1, t_2, t_4, t_5 in Eq. 6 are uniquely related to the coefficients α, β, δ, and ϵ in Eq. 6. Values of these parameters for the different model choices can be found in Tab. I.

	α (MeV)	β (MeV)	γ	δ (MeV)	$\varepsilon\left(\frac{c^2}{\mathrm{GeV}^2}\right)$	K (MeV)
SM	-390	320	1.14	1.57	500	200
HM	-130	59	2.09	1.57	500	376

TABLE I. Parameter sets for the nuclear equation of state used in the IQMD model

The parameters ϵ and δ are given by fits to the optical potential extracted from elastic scattering data in pA collisions[16, 17]. Two of the 3 remaining parameters of the ansatz are fixed by the condition that the volume energy has a minimum of $E/A(\rho_0) = -16$ MeV at ρ_0.

The third parameter is historically expressed as the compression modulus K of nuclear matter, which corresponds to the curvature of the volume energy at $\rho = \rho_0$ (for $T=0$) and is also given in Tab. I

$$K = -V\frac{\partial p}{\partial V} = 9\rho^2 \frac{\partial^2 E/A(\rho)}{(\partial\rho)^2}|_{\rho=\rho_0} \quad . \tag{7}$$

An equation of state with a rather low value of the compression modulus K yields a weak repulsion of compressed nuclear matter and thus describes "soft" matter (denoted by "SM"). A high value of K causes a strong repulsion of nuclear matter under compression (called a "hard EoS", HM).

III. SURVEY OF THE REACTION

Motivated by the good agreement between theory and experiment in most relevant flow observables [1, 8], we use the theoretical model in order to understand the reaction in its full complexity. We start with the time

evolution of the heavy ion reaction Au+Au at E_{kin} = 1.5 $AGeV$ and an impact parameter b=6 fm. In Fig. 2 the density profile of protons, ($\rho_{yx} = \frac{1}{N_{event}} \int \frac{dN_p}{dxdydz} dz$) at 0.1, 0.5, 1.0 t_{pass} is shown, where t_{pass} is the time the projectile would need to pass by the target assuming that both continue with their initial velocity, i.e. t_{pass} =22.9 fm/c for Au+Au at E_{kin} = 0.6 $AGeV$ and 16.9 fm/c for E_{kin} = 1.5 $AGeV$. After t_{pass} the spectator matter (those nucleons of projectile and target which are outside of the overlap of projectile and target) can absorb no more nucleons from the participant region (the nucleons of the overlap region of projectile and target). We display from top to bottom the projection of all nucleons onto the zx plan (where x is the direction of the impact parameter and z the direction of the beam), onto the zy plane and onto the xy plane for three different times (0.1, 0.5 and 1 times the passing time). As can be seen in the top figures the central (participant) matter is highly compressed when the overlap of the colliding system is largest (at t=0.5 t_{pass}), i.e. when the spectator matter is situated closest to the participants. The amount of stopping in such a reaction is insufficient to form a combined system. Rather projectile and target remnants separate but they are connected for quite a while by a ridge with a quite high particle density. This ridge will disintegrate when projectile and target remnants separate further. The importance of this ridge can be seen in the second line which shows the density profile in the zy plane. Even at t_{pass} we find the highest density at z=0 and therefore in the ridge. We see clearly in the bottom panels that the center of the spectator remnant has a larger x value than the impact parameter. This shows how the repulsive potential interaction at high densities creates a large v_1 value, i.e. a large in-plane flow.

The choice of the EOS influences the reaction scenario calculated by the model. This can be studied in detail by evaluating the difference (SM-HM) of the proton densities projected onto the xy plane, $\Delta\rho_{xy} = \frac{1}{N_{event}} \int \frac{dN_p^{SM}}{dxdydz} dz - \frac{1}{N_{event}} \int \frac{dN_p^{HM}}{dxdydz} dz$, and correspondingly onto the zx and the zy planes. The results are shown in Figs. 3 and 4. The red color signals regions in which a soft EoS yields a higher density, whereas the blue color marks the regions in which the density is higher for a hard EoS. Fig. 3 (4) displays this density difference at t = 1.0 t_{pass} in coordinate (momentum) space for the reaction Au+Au at 0.6 AGeV (left) and at 1.5 AGeV (right) incident energy and the impact parameter b=6 fm. The density of protons in the geometrical overlap region of projectile and target is substantially higher for a soft EoS, as can be seen in the panels, whereas at larger distances from the reaction center we observe a higher density for a hard EoS. This surplus in the density for a hard EOS in the xy plane at .6 $AGeV$ is more important in x-direction, but it becomes rather isotropic at 1.5 AGeV. The origin of this surplus in x-direction is rather different from that in y-direction: in the middle panel it is shown that the surplus in x-direction has its

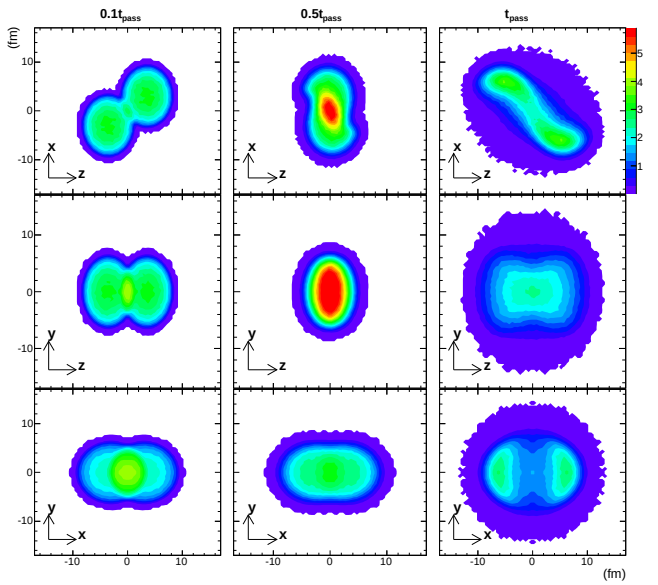

FIG. 2. (Color online) Time evolution of the proton density profile ($\frac{dN}{dxdy}$ in $event^{-1} fm^{-2}$) in the reaction ^{197}Au+^{197}Au at 1.5 AGeV incident energy, b= 6 fm, soft (SM) EoS, in the zx(top) zy (middle) and xy (bottom) planes. We present the density profile at the times 2, 8 and 16 fm/c (0.1, 0.5, 1.0 t_{pass} respectively) in the left, central and right columns respectively.

origin in the in-plane flow of the spectator matter or in a finite v_1 coefficient in eq. 1. This in-plane flow is considerably stronger for a hard EoS as compared to a soft EoS [17–19]. In y-direction the surplus in density of the hard EoS is concentrated at around z=0 (lower panels) and is created by particles which are stopped completely ($p_z \approx 0$) in the center of mass of the reaction. Their emission is caused by a stronger density gradient (and hence a stronger force) in y-direction for a hard (HM) EoS as compared to a soft (SM) one. We will come back to this point later.

In order to analyze the model results in momentum space we introduce the four-velocity u with the transverse component $u_t = \beta_t \gamma$. The 3-vector β is the velocity in units of the light velocity and $\gamma = 1/\sqrt{1-\beta^2}$. Throughout we use scaled units $y_0 = y/y_p$ and $u_{t0} = u_t/u_p$, with $u_p = \beta_p \gamma_p$, the index p referring to the incident projectile in the c.o.m.. In these units the initial target-projectile rapidity gap always extends from $y_0 = -1$ to $y_0 = 1$.

In momentum space (Fig. 4) we observe a complementary distribution. In the xy plane (upper panels) the acceleration of protons in x direction is very modest for a soft (SM) EOS but the stronger in-plane flow for a hard EoS yields a larger velocity in x-direction (middle panels). The soft EoS leads also to less stopping, as can be seen in the lower panels. At both energies projectile and target do not form an equilibrated source at midrapidity but separate rather quickly as can be also seen from fig. 2. In Fig.5 fast moving particles around midrapidity

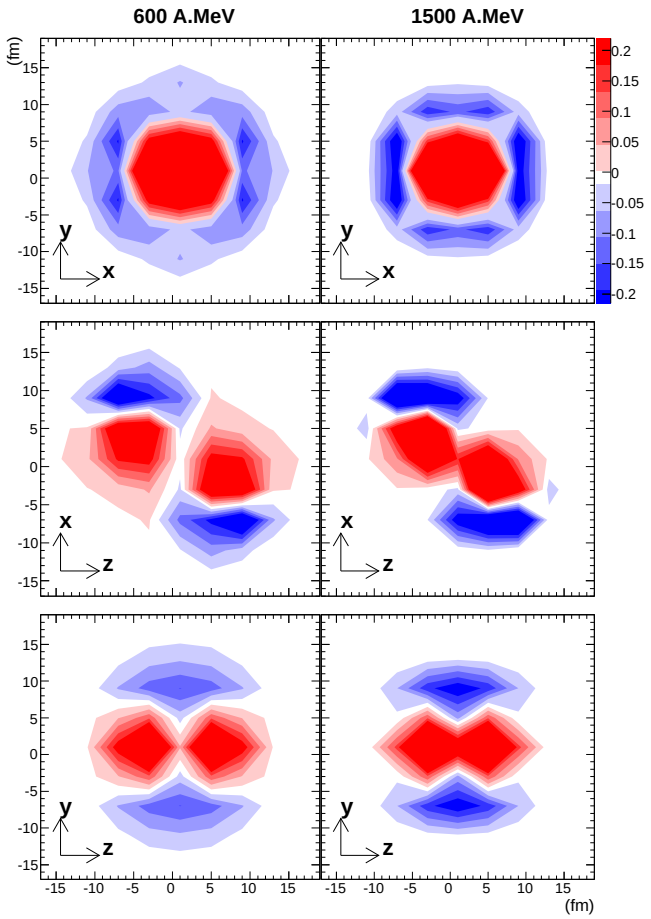

FIG. 3. (Color online) Difference of the proton density profiles ($\frac{\delta(N_{SM}-N_{HM})}{dxdy}$ in $event^{-1}fm^{-2}$) between a soft (SM) and a hard (HM) EoS in the (from top to bottom) xy, zx and zy planes. Predictions for $^{197}Au+^{197}Au$ at 0.6 AGeV and 1.5 AGeV incident energies are shown on the left and columns respectively. The impact parameter is 6 fm and the model results are for $t = t_{pass}$.

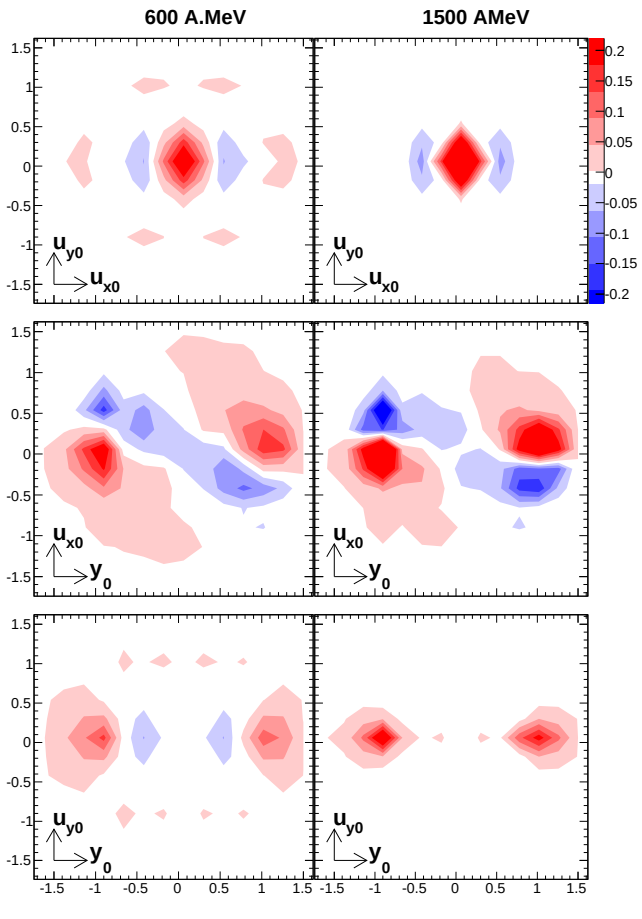

FIG. 4. (Color online)Same as Fig. 3 but expressed in the scaled quantities in the (u_{x0}, u_{y0}), (u_{x0}, y_0), (u_{y0}, y_0) (see text).

have been selected ($|y_0| < 0.2$, $u_{t0} > 0.4$. Those cuts have also been used in the FOPI analysis [8]). The density difference distribution in the xy plane shown Fig.5 for two energies and two reaction times is rather different compared to the distribution of all particles, Fig.3. The filter removes spectator and participant protons with low velocities. Hence, the surplus of particles emitted in x-direction is not visible anymore but only the particle excess in y-direction. Comparing the left (at t_{pass}) and right panels (at $2t_{pass}$) we see that these particles have indeed a large velocity in y-direction as can be seen from the large distance the particle travel between t_{pass} and $2t_{pass}$. For a soft EoS the fast fireball particles in the center of the reaction are more numerous. These fast particles do not expand very differently as compared to the slower ones.

Fig. 6 shows the averaged reduced nuclear density (ρ/ρ_0) around the selected nucleons ($|y_0| < 0.2$,$u_{t0} > 0.4$) in the xy plane (upper four panels) and in the zx plane (lower four panels) for incident energies 0.6 and 1.5 AGeV at $t = 0.5t_{pass}$ (left column) and $t = 0.5t_{pass}$ (right column). The density profiles have been integrated over the third dimension. We confront the average density around those nucleons which are emitted with ($|y_0| < 0.2$) and which have a transverse velocity ($u_{t0} > 0.4$) (color coded) with that of all nucleons (lines). At half the passing time a difference has not developed yet. At passing time we see in the right upper panels the consequences of the in plane flow v_1. The majority of particles has moved to larger x values whereas the particle emitted at midrapidity have a more isotropic emission pattern and the density around these particles shows almost an azimuthal isotropy. The high density zone has at $t_{pass}/2$ an almost almond shaped form but - in contradistinction to higher energies - the energy density is not that high that this yields a positive v_2. In the zx plane we see that the midrapidity baryons are coming from the ridge between projectile and target. The higher the energy the higher is the density of this ridge.

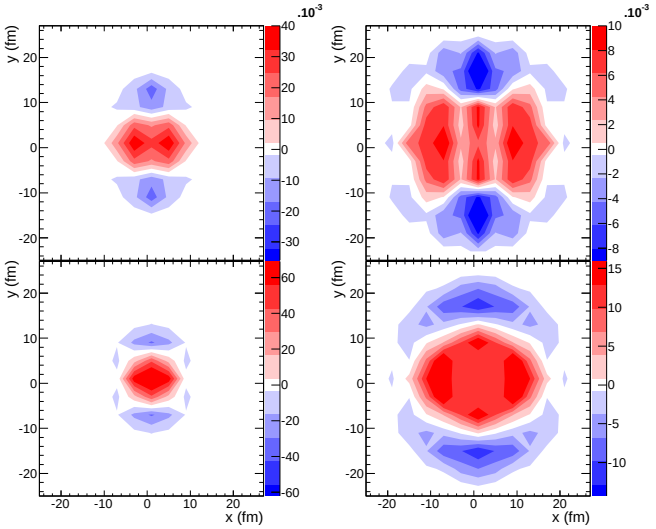

FIG. 5. (Color online) Difference between a soft (SM) and a hard (HM) EoS of the density profiles of protons emitted finally at mid-rapidity ($|y_0| < 0.2$) and with a high transverse velocity ($u_{t0} > 0.4$), in reactions in the xy plane. We display the predictions of ^{197}Au+^{197}Au at 0.6 AGeV (top) and 1.5 AGeV (bottom) incident energies, b = 6 fm, at t_{pass} (left) and $2t_{pass}$ (right).

IV. THE ELLIPTIC FLOW

Fig. 7 shows the time evolution of the elliptic flow $v_2(t) =< \frac{p_x^2(t)-p_y^2(t)}{p_x^2(t)+p_y^2(t)} >$ of protons in the Au+Au collisions at 0.6 (top) and 1.5 (bottom) AGeV for SM (red) and HM (blue). For both equations of state v_2 is negative means that the momentum in the out of plane direction is larger than in plane. This phenomenon is called "squeeze" and appears also in hydrodynamical calculations. Selecting protons emerging with a high transverse velocity $u_{t0} > 0.4$ (dashed curves) enhances its amplitude. The value of v_2 at midrapidity depends strongly on the EoS, although, in both cases it is only few percent of the modulus. At the passing time, t_{pass}, the difference between a soft and a hard equation of state has already reached its asymptotic value.

In the simulations one can follow how v_2 develops as a function of time. In particular, it is possible to distinguish the time evolution of the momentum change due to collisions and due to the potential interactions. This is achieved by recording the momenta of the protons before and after each collision and before and after every time step during which the proton propagates in the potential created by all other nucleons. Figs. 8 and 9 give an overview of the transverse momentum flow at beam energies of 0.6 $AMeV$ and 1.5 $AGeV$, respectively. We display the average transverse momentum transfer which the nucleons have suffered as a function of their position, up to half the passing time (top) and until passing time (bottom), after integration over the z-(beam) direction.

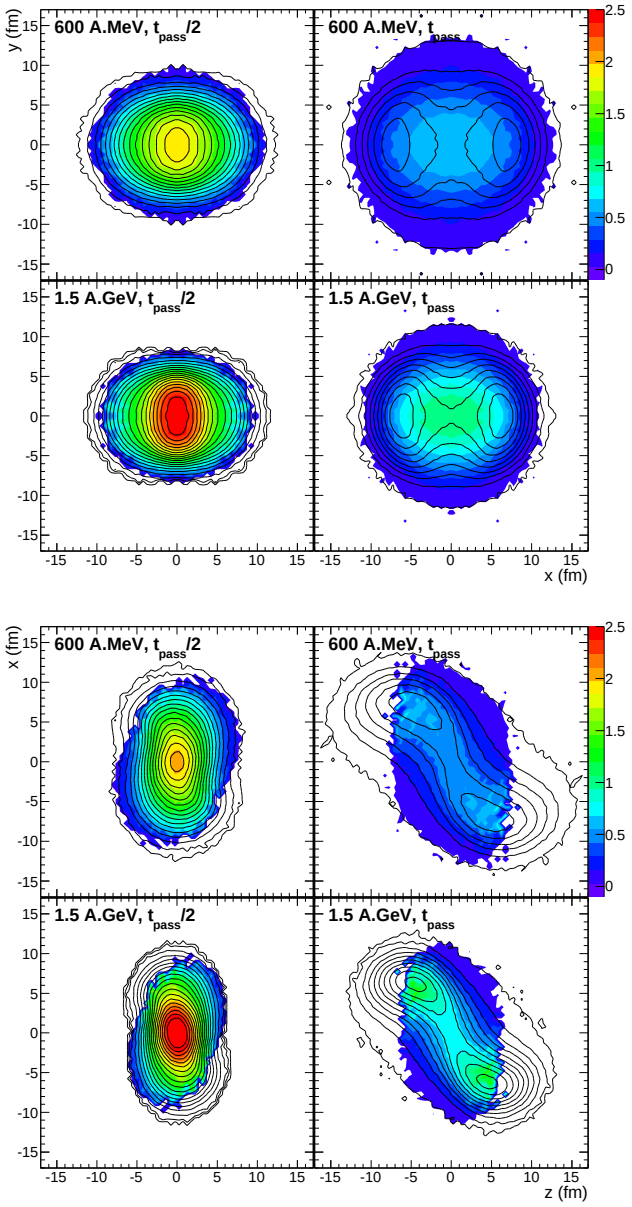

FIG. 6. (Color online) Distribution of the mean baryonic reduced density (ρ/ρ_0) around the selected protons in the ^{197}Au+^{197}Au collisions, b=6 fm, at 0.6 (top) and 1.5 (bottom) AGeV incident energies, at 2 different times: at full overlap of the system (half passing time, left) and at the passing time (right). Black lines and colored contours correspond to all protons and to those finally emitted at mid-rapidity ($|y_0| < 0.2$) with a high transverse velocity ($u_{t0} > 0.4$), respectively. On the left 4 panel we projected on the transverse xy plane, on the right 4 panels on the zx plane.

The left panels show the transverse momentum change due collisions, the right hand side due to potential interactions. Until half passing time t_{pass} the collisions and potential interactions have created the largest momentum transfers in the overlap zone of projectile and target, in addition, the potential is responsible for a

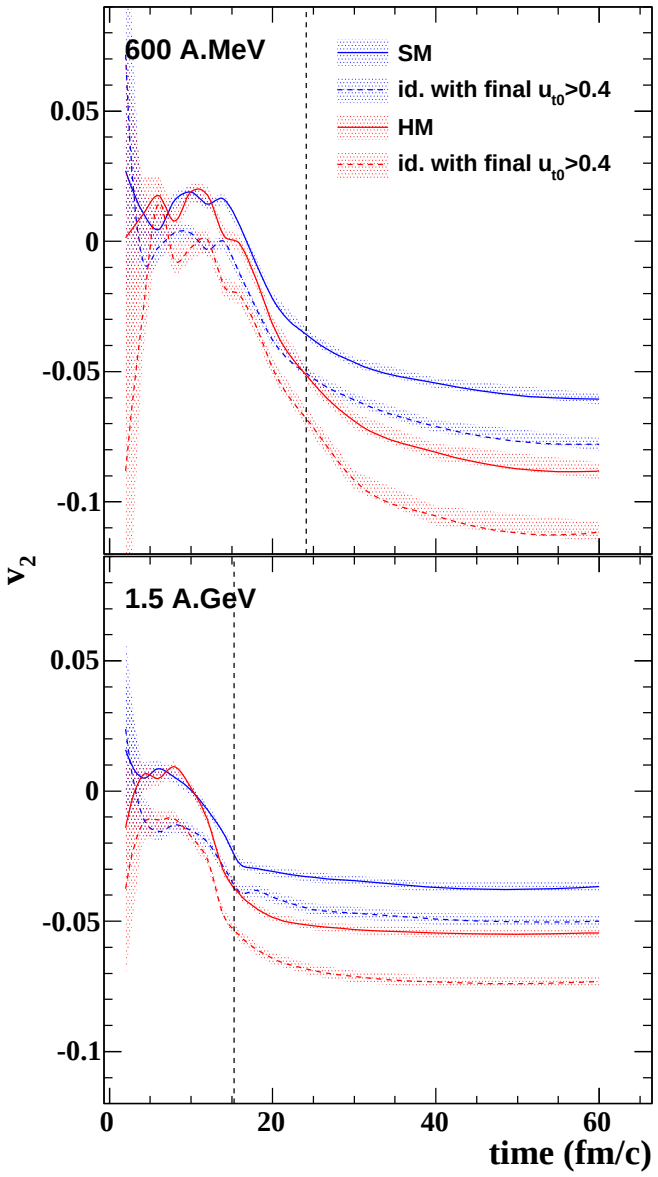

FIG. 7. (Color online) Time evolution of the elliptic flow $v_2(t) = \frac{p_x^2(t)-p_y^2(t)}{p_x^2(t)+p_y^2(t)}$ of protons at midrapidity in the ^{197}Au+^{197}Au collisions at 0.6 (top) and 1.5 (bottom) A.GeV incident energies, b=6 fm. We show the results with a hard (HM, red lines) and a soft (SM, blue lines) EoS, and with (dashed lines) or without (full lines) excluding the protons having finally a low transverse velocity $u_{t0} \leq 0.4$. The dashed vertical lines indicate the passing time.

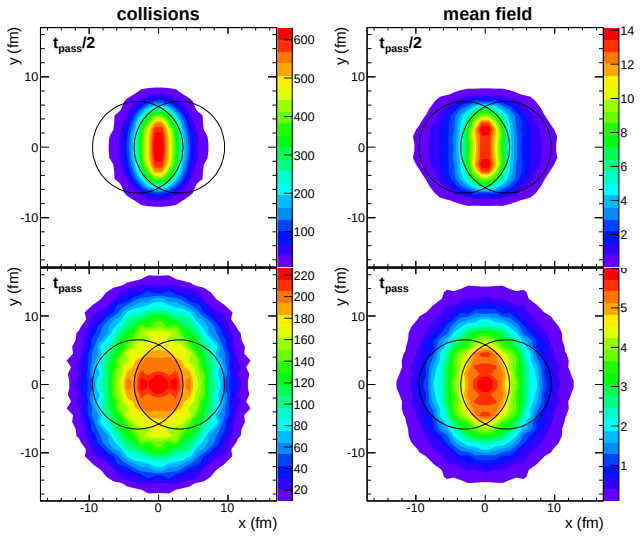

FIG. 8. (Color online) IQMD (with SM EoS) predictions for the mid-peripheral (b=6 fm) collisions of ^{197}Au+^{197}Au at 0.6, at two times: half t_{pass} (maximal overlap) and t_{pass} (top and bottom panels respectively). The panels display $\Delta P_t(t) = \sqrt{(p_x(t)-p_x(t=0))^2+(p_y(t)-p_y(t=0))^2}$ (in arbitrary units) as a function of (x,y). Only protons being finally at mid-rapidity ($|y_0| < 0.2$) are selected here. The left and right panels show respectively the momentum transfer due to collisions and to the mean field. The superimposed circles show the spatial extension of the incoming projectile and target in this plane.

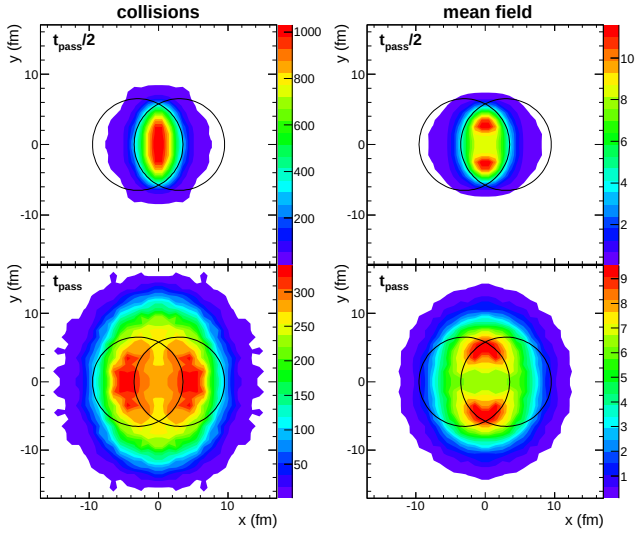

FIG. 9. (Color online) Same as Fig. 8 for 1.5 A.GeV incident energy.

large momentum transfer into the out of plane direction. This is especially seen for the 1.5 $A.GeV$ reaction. This strong acceleration and the consequently large momentum transfer in y-direction is, as we will see, at the origin of the dependence of v_2 on the nuclear EoS. At passing time t_{pass}, we note that those nucleons have the largest momentum transfers due to collisions which have entered the spectator matter because they experience more collisions. A strong mean field momentum transfer we observe for $E_{beam} = 1.5\ AGeV$ at x=0 and y values close to the surface of the nuclei. Here the overlap region of projectile and target reaches a density close to twice normal

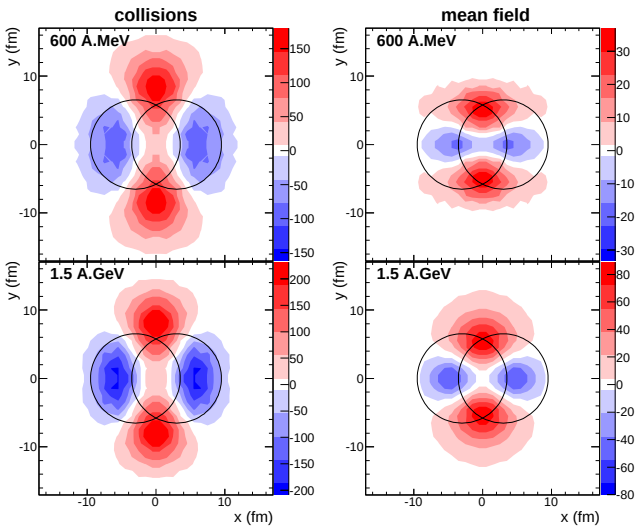

FIG. 10. (Color online) IQMD (with SM EoS) predictions for the mid-peripheral (b=6 fm) collisions of ^{197}Au+^{197}Au at 0.6 (top panels) and 1.5 (bottom panels) A.GeV incident energy, at passing time. The panels show the mean difference (arbitrary unit) between the out-of-plane (y axis) and in-plane (x axis) of the momentum change (up to time $t = t_{pass}$) since the beginning of the collision $< \Delta p_y(t) - \Delta p_x(t) >$ separately due to the collisions (left panels) and to the mean field (right panels), in the xy plane (transversal to the projectile velocity). The sign of the momentum change is defined by its orientation relative to the momentum vector at t: $\Delta p_i(t) = \Delta\vec{p_i}(t).\frac{p_i\vec{(t)}}{|p_i\vec{(t)}|}$ Only protons observed finally at mid-rapidity ($|y_0| < 0.2$) are selected here. The superimposed circles show the maximum spatial extension of the incoming projectile and target on this plane.

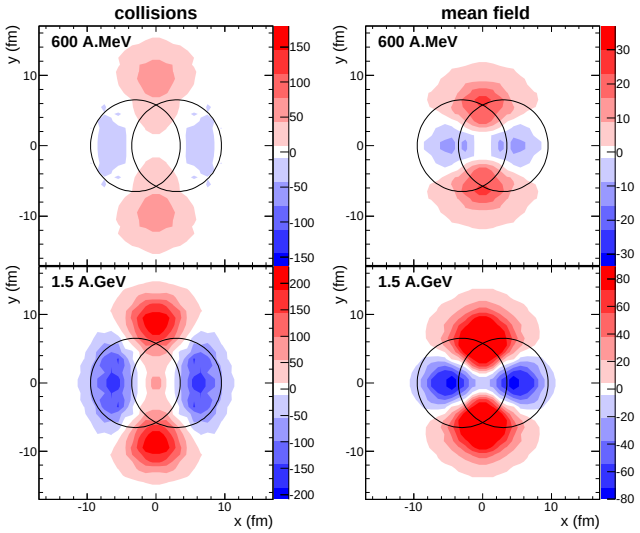

FIG. 11. (Color online) Same as Fig. 10 with HM EoS.

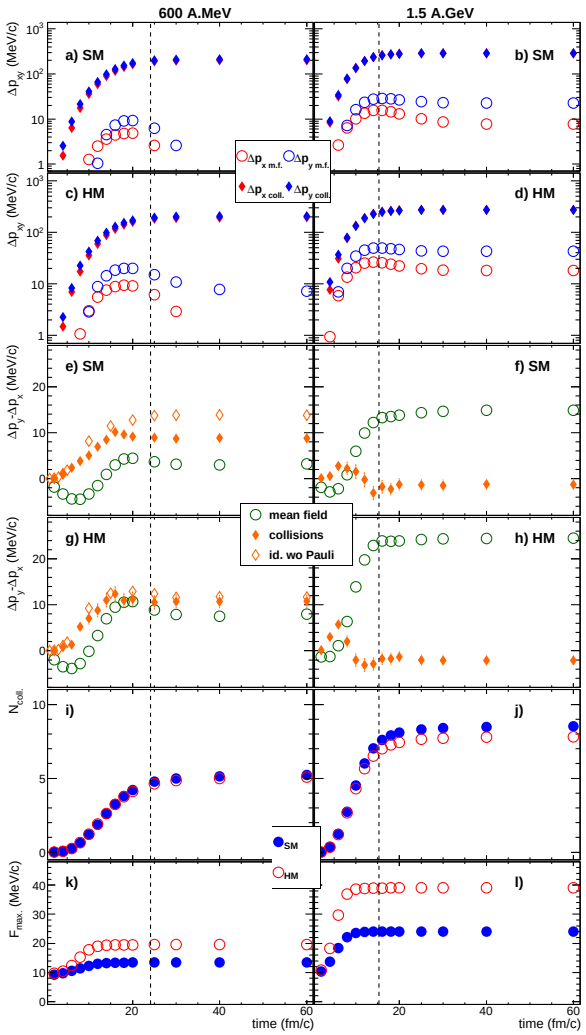

FIG. 12. Same event selection as in Fig. 10. Time evolution of various observables. Left and right panels show results at 600 and 1500 A.MeV incident energies respectively. Panels a, b: show for the SM EoS the integrated momentum transfer in x (red symbols) and y (blue symbols) directions, caused by the mean field (m.f., open circles) and by collisions (coll., diamonds). Panels c and d: *idem* for the HM EoS. Panels e and f: show for the SM EoS the integrated difference between the out-of-plane (y) and in-plane (x) contribution of the momentum transfer from the mean field (green open circles) and from the collisions with (orange full diamonds) or without (orange empty diamonds) Pauli blocking. Panels g and h: *idem* for the HM EoS. Panels i and j: number of collisions suffered by the selected protons comparing the SM (blue circles) and HM (red squares) EoS's. Panels k and l: *idem* with the maximum undergone force due to the mean field. The vertical dashed lines indicate the passing time.

nuclear matter density and therefore the density gradient with respect to the surrounding vacuum is large. Because the force is proportional to the density gradient we observe here the strongest forces.

Figs. 10 and 11 show this situation from a different point of view. Here we display $< \Delta p_y(t) - \Delta p_x(t) >$

with $\Delta p_i(t) = \Delta\vec{p_i}(t).\frac{\vec{p_i}(t)}{|\vec{p_i}(t)|}$ for a soft (SM) EoS (Fig. 10) and for a hard (HM) EoS (Fig. 11). On the top (bottom) panels of each figure this quantity is shown for $E_{kin} = 0.6\ AGeV (1.5\ AGeV)$, at t_{pass}. The left panels show the momentum transfer due to collisions, the right panels due to potential interactions. If we compare the momentum transfer due to collisions we see a very similar pattern for SM and HM and hence for the difference. The absolute magnitude his, however, quite different. A much larger difference is observed for the momentum transfer due to the potential interaction. Here the HM EoS pushed the matter much more into the x as well as into the y direction than the SM EoS. The region with large momentum transfers is much more extended and the absolute value is larger.

The quantitative result of this analysis, the integrated change of the x and y momentum due to collisions and the potential interaction, is presented in Fig.12 for $^{197}Au+^{197}Au$, b= 6 fm, and $E_{kin} = 0.6\ AGeV (1.5\ AGeV)$. In row a) and c) the total momentum changes $|\Delta P_x|$ and $|\Delta P_y|$ due to collisions and potential interactions are shown for a soft (upper row) and a hard EOS (lower row), in row e) and g) we present $\Delta P_y - \Delta P_x$. For both EoS, SM and HM, the total momentum change due to collisions is much larger than that due to the potential, but the momentum change in x-direction and in y- direction are quite similar. If one calculates the difference of the momentum change, $\Delta P_y - \Delta P_x$, one observes that for a soft EoS the collisions contribute more than the potential (panels e) and f)), whereas for a hard EoS both contribute about the same (panels g) and h)). The contribution of the collisions to $\Delta P_y - \Delta P_x$ is rather independent of the EoS, as one can see comparing panels e) and g) for 0.6 AGeV and f) and h) for 1.5 AGeV. Therefore, the EoS dependence of $\Delta P_y - \Delta P_x$ comes almost exclusively from potential interaction. This is the seminal result of our analysis. The participant nucleons getting stopped by collisions with the in-plane spectator matter contribute to v_2 but they are not at the origin of the EoS dependence of v_2. Collisions contribute about 50% for a hard EoS and about 70% for a soft EoS to $\Delta P_y - \Delta P_x$.

Row i) shows how the integrated number of baryon collisions increases as a function of time whereas in row k) it is shown how the integrated average maximal force which the nucleons have experienced is depending on t. We see clearly that the forces are strongest close to $t = t_{pass}/2$ and there is almost a factor of two difference between a soft (SM) and a hard (HM) equation of state.

The origin of the EoS dependence of v_2 can be further investigated by analysing the elliptic flow in the xy plane as a function of the transversal distance from the center of the reaction determined at t_{pass}. This is done in Fig. 13 selecting protons emerging finally in the midrapidity region $|y_0 < 0.2|$. We imposed in addition that they finally have a high transverse velocity u_{t0} which only enhances the amplitude of the observed phenomena, as seen in Fig. 7. Whereas the outer nucleons ($R_{xy} > 4fm$)

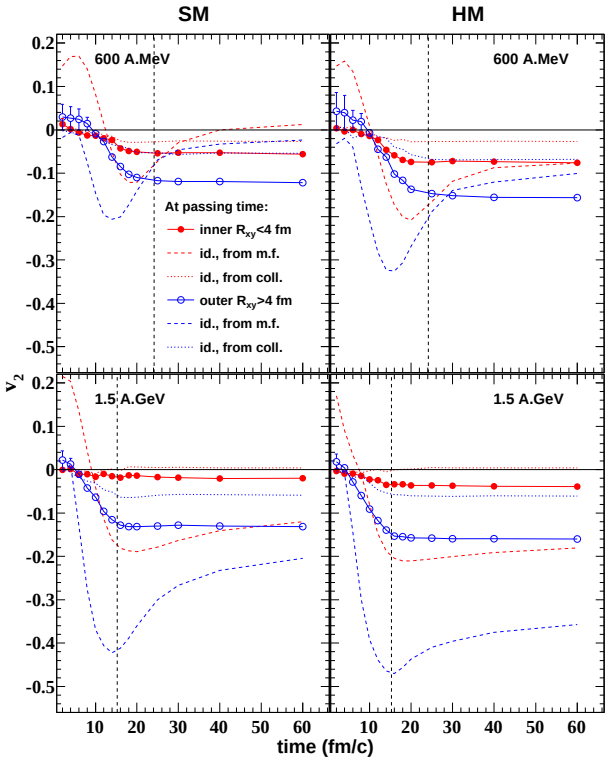

FIG. 13. (Color online) Time evolution of the elliptic flow, v_2, of protons finally emitted at mid-rapidity ($|y_0| < 0.2$) with a large transverse velocity $u_{t0} > 0.4$ in the $^{197}Au+^{197}Au$ collisions, b=6 fm, at 0.6 (top) and 1.5 (bottom) AGeV incident energies, with a soft (SM, right) and a hard (HM, left) EoS. The protons situated, at the passing time, transversally close (radial distance to the centre of the collision on the transversal plane $R_{xy} < 4fm$) or far ($R_{xy} > 4fm$) to/from the main axis of the collision are distinguished respectively by red and blue lines. The overall v_2 (symbols) is detailed into its two contributions: the v_2 developed by the momentum transfer due to the mean field and the collisions, respectively depicted by dashed and dotted lines. Black vertical dashed lines indicate the passing time.

develop a strong negative v_2, at the higher energy the inner part ($R_{xy} < 4$ fm) expands inside the error bars isotropically in azimuthal direction, however, there is a small contribution to negative v_2 at low energies. The asymptotic v_2 values are reached quite fast, already at $t/t_{pass} = 1$ (dashed line). This observation is very different from that at ultra relativistic energies where the highly compressed overlap region develops a positive v_2 which is proportional to the eccentricity of the almond shaped overlap region. Here, at lower beam energies, the internal movement due to the Fermi motion and due to the fact that density gradients are not negligible as compared to the beam momentum and therefore the nucleons can react to the sudden increase in density while projectile and target are passing. The higher the beam energy the less the internal motion can change the source shape - which becomes therefore almond shaped at high beam

energies. The internal motion provokes that at lower energies the outer part of high density region is not almond shaped but almost spherical whereas the central part has an approximate almond shape form but the energy density is not sufficiently high to convert this into a positive v_2. The higher the beam energy the more energy is stored in this overlap region. We conclude that with increasing beam energy v_2 becomes positive as also observed experimentally.

The excitation function of the elliptic flow of protons at mid-rapidity in $^{197}Au+^{197}Au$ at b=4 fm is shown in Fig. 14 with various conditions on their final transverse velocity: all values, $u_{t0} > 0.4$ and $u_{t0} > 0.8$ (respectively from the top to the bottom panels). Results with a soft (SM, blue lines) and a hard (HM, red lines) EoS differ largely above 400 A.MeV beam energy. We observe in addition a strong change of the elliptic flow with the incident energy in this regime, a maximum being reached around 600 A.MeV. The strength of v_2 is enhanced when focusing on large transverse velocity protons. Comparing with experimental observations [8] done around the same impact parameter for protons having a high $u_{t0} > 0.8$, we find a good agreement using the soft (SM) EoS (lowest panel in Fig. 14). There, both the amplitude and the evolution of the elliptic flow with the bombarding energy are well reproduced by the model.

From this analysis we can conclude that the elliptic flow observed in the reactions around $E_{kin} \approx 1AGeV$ for protons at mid-rapidity ($|y_0| < 0.2$) has two origins: Firstly, it is created by collisions of participant nucleons with the spectator matter (collisional contribution). This component of v_2 is almost independent of the EoS but in the case of a hard EoS as large as as the second contribution, the potential contribution. For a soft EoS the potential contribution is reduced by roughly 50%. A soft EoS (SM) is in better agreement with the data than a hard equation of state (SM). The potential contribution is created because those protons which are close to the surface of the interaction zone in y-direction get accelerated out of the reaction plane due to a strong density gradient in this direction whereas protons close to the surface of the interaction zone in x-direction see a much smaller density gradient due to the presence of the spectator matter. This effect is amplified if one selects particles with a high transverse velocity, $u_{t0} > 0.4$.

V. SUMMARY

We analysed the origin of the experimentally observed negative elliptic flow which develops at mid-rapidity in heavy ion reactions in the $E_{kin} \approx 1AGeV$ region. QMD calculations have shown that this elliptic flow depends stronger on the nuclear EoS than any other observable investigated so far. We have demonstrated that the EoS dependence of this negative v_2 is created by nucleons which are situated on the outer part of the overlap region of projectile and target. Between the maximum overlap and

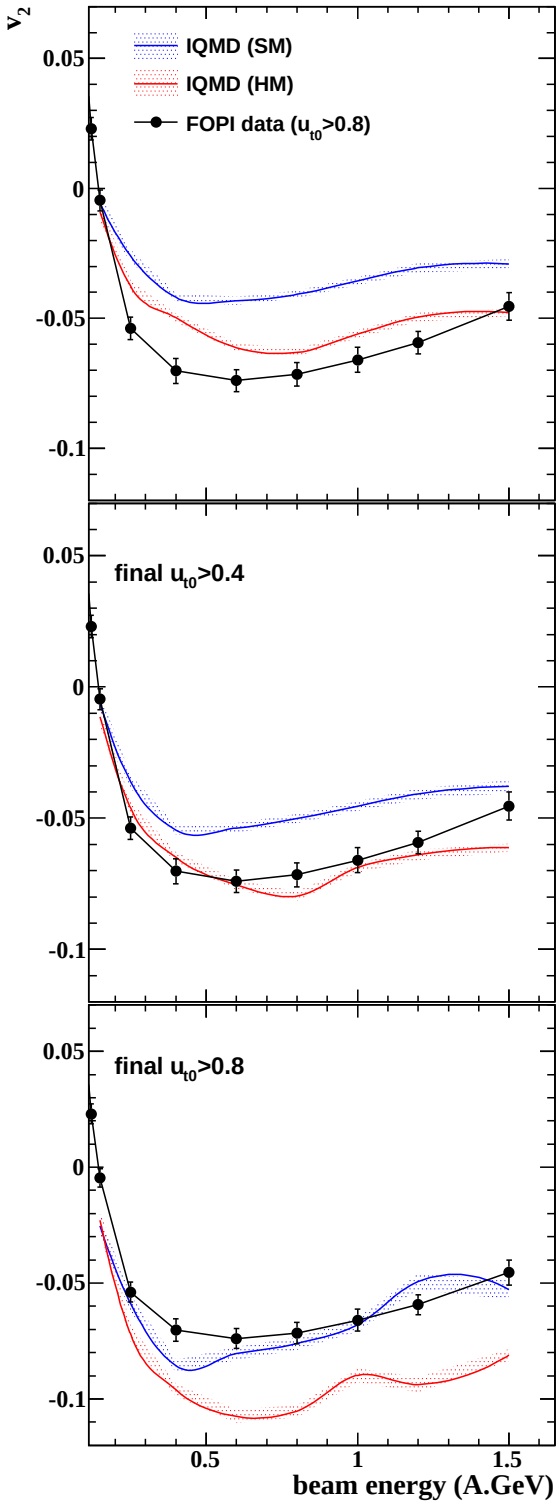

FIG. 14. (Colour online) Excitation function of the elliptic flow of protons at mid-rapidity (top panel) and with the additional constraints $u_{t0} > 0.4$ and $u_{t0} > 0.8$ (middle and bottom panels respectively) calculated with a SM (blue) and HM (red) EoS in $^{197}Au+^{197}Au$ collisions at an impact parameter of $b = 4\ fm$. Errors on mean values are shown by the greyed areas. IQMD predictions are compared with experimental data of the FOPI collaboration shown in Fig. 29 of Ref. [8], extracted for $3.1fm < b < 5.6fm$ with $u_{t0} > 0.8$.

the passing time these nucleons experience a weaker density gradient in the reaction plane as compared to out of the reaction plane, due to the presence of the spectators. This translates into a stronger force into the y-direction. The density gradients and consequently the forces are stronger for a hard EoS (HM) as compared to a soft one (SM). This explains quantitatively the dependence of v_2 on the hadronic EoS. The scattering of participant protons with the spectator matter produces an elliptic flow as well, but this component is almost independent on the EoS. The agreement of the QMD calculations with data for a soft EoS adds to the circumstantial evidence that the soft EoS describes correctly the matter at a density obtained by beam energies of the order of 1 AGeV, an observation that has already been made by analysing the K^+ production data [12, 14].

Acknowledgments: We acknowledge fruitful discussions with W. Reisdorf.

[1] A. Le Fèvre, Y. Leifels, W. Reisdorf, J. Aichelin and C. Hartnack, arXiv:1501.05246 [nucl-ex].
[2] H. Stoecker, L. P. Csernai, G. Graebner, G. Buchwald, H. Kruse, R. Y. Cusson, J. A. Maruhn and W. Greiner, Phys. Rev. C **25** (1982) 1873.
[3] G. Buchwald, G. Graebner, J. Theis, J. Maruhn, W. Greiner, H. Stoecker, K. A. Frankel and M. Gyulassy, Phys. Rev. C **28** (1983) 2349.
[4] H. Stoecker and W. Greiner, Phys. Rept. **137** (1986) 277.
[5] H. H. Gutbrod, K. H. Kampert, B. Kolb, A. M. Poskanzer, H. G. Ritter, R. Schicker and H. R. Schmidt, Phys. Rev. C **42** (1990) 640.
[6] M. Luzum and P. Romatschke, Phys. Rev. Lett. **103** (2009) 262302 [arXiv:0901.4588 [nucl-th]].
[7] C. Pinkenburg *et al.* [E895 Collaboration], Phys. Rev. Lett. **83** (1999) 1295 [nucl-ex/9903010].
[8] W. Reisdorf *et al.* [FOPI Collaboration], Nucl. Phys. A **876** (2012) 1 [arXiv:1112.3180 [nucl-ex]].
[9] A. Andronic *et al.* [FOPI Collaboration], Phys. Lett. B **612** (2005) 173 [nucl-ex/0411024].
[10] A. Andronic, J. Lukasik, W. Reisdorf and W. Trautmann, Eur. Phys. J. A **30** (2006) 31 [nucl-ex/0608015].
[11] P. Danielewicz, R. Lacey and W. G. Lynch, Science **298** (2002) 1592 [nucl-th/0208016].
[12] C. Hartnack, H. Oeschler and J. Aichelin, Phys. Rev. Lett. **96** (2006) 012302 [nucl-th/0506087].
[13] J. Aichelin, Phys. Rept. **202** (1991) 233.
[14] C. Hartnack, H. Oeschler, Y. Leifels, E. L. Bratkovskaya and J. Aichelin, Phys. Rept. **510** (2012) 119 [arXiv:1106.2083 [nucl-th]].
[15] C. Hartnack, R. K. Puri, J. Aichelin, J. Konopka, S. A. Bass, H. Stoecker and W. Greiner, Eur. Phys. J. A **1** (1998) 151 [nucl-th/9811015].
[16] S. Hama, B. C. Clark, E. D. Cooper, H. S. Sherif and R. L. Mercer, Phys. Rev. C **41** (1990) 2737.
[17] J. Aichelin, A. Rosenhauer, G. Peilert, H. Stoecker and W. Greiner, Phys. Rev. Lett. **58** (1987) 1926.
[18] G. Peilert, H. Stoecker, W. Greiner, A. Rosenhauer, A. Bohnet and J. Aichelin, Phys. Rev. C **39** (1989) 1402.
[19] C. Hartnack and J. Aichelin, Phys. Lett. B **506** (2001) 261 [nucl-th/9901087].